A system analysis and image reconstruction tool for optoacoustic imaging with finite-aperture detectors

Yiyong Han*[a,b], Vasilis Ntziachristos[a,b], and Amir Rosenthal[a,b]

[a]Institute for Biological and Medical Imaging, Helmholtz Zentrum Muenchen, Ingolstaedter Landstrasse 1, 85764 Neuherberg, Germany; [b]Chair for Biological Imaging Technische Universitaet Muenchen, Ismaningerstraße 22, 81675 Muenchen, Germany

*hanyiyong@gmail.com; phone +49-89-31871247; fax +49-89-31873017

ABSTRACT

Model-based optoacoustic reconstruction can incorporate the shape of transducers. However, the accompanying memory cost will hinder it for high resolution performance. The propose method provides over an order of magnitude reduction in inversion time in experiments. Additionally, it also suits for the analysis of inversion stability.

Keywords: optoacoustic tomography, photoacoustic tomography, reconstruction algorithms, inverse problems, wavelet packet, regularization.

1. INTRODUCTION

Finite-aperture detectors are commonly used in optoacoustic tomography [1-2]. Unlike typical back-projection [3], model-based reconstruction incorporating the finite size of transducers will achieve better quantification [4]. However, large matrix size and long computational time will hinder it for high resolution performance. In this paper, generalized wavelet packet interpolated-model-matrix-inversion (IMMI) algorithm with finite-aperture detectors (GWP-IMMI-FAD) is proposed and demonstrated in 2D for line-segment detectors using experimental data. Additionally, our framework is demonstrated for the analysis of inversion stability and reveals a new, non-monotonic dependency of the system condition number on the detector size.

2. THEORETICAL BACKGROUND

In a typical optoacoustic imaging setup, in which nanosecond laser pulses are used and the acoustic medium is assumed to be homogeneous, the pressure measured by the acoustic detector $p(r,t)$ is often modeled by the following integral equation: [2, 5]

$$p(r,t) = \frac{\Gamma}{4\pi v}\frac{\partial}{\partial t}\int_{|\Delta r|=vt}\frac{H_r(r-\Delta r)}{vt}ds\,, \tag{1}$$

where v is the speed of sound in the medium; Γ is the Grueneisen parameter; $H_r(r)$ is the amount of energy absorbed in the tissue per unit volume; s is the spherical surface; $|\Delta r|$ equals to v times t. In the case of a finite-aperture detector, the response of the detector $p_{\det}(t)$ is obtained by integrating $p(r,t)$ over the surface of the detector S:

$$p_{\det}(t) = \int_{r\in S} p(r,t)dS\,. \tag{2}$$

The discretization of Eq. (2) leads to the following matrix relation:

$$\mathbf{p} = \mathbf{Mz}\,, \tag{3}$$

where $\mathbf{p}$ is a column vector representing the measured acoustic waves at various detector positions and time instants; $\mathbf{z}$ is a column vector representing the object values; $\mathbf{M}$ is the forward model matrix.

The reconstruction problem involves inverting the matrix relation in Eq. (3). When $\mathbf{M}$ is well-conditioned, inversion may be performed by least squares solution:

Opto-Acoustic Methods and Applications in Biophotonics II, edited by Vasilis Ntziachristos, Roger Zemp, Proc. of SPIE Vol. 9539, 953915 · © 2015 SPIE · CCC code: 1605-7422/15/$18 · doi: 10.1117/12.2183811

$$\mathbf{z} = \arg\min \|\mathbf{p} - \mathbf{Mz}\|_2^2 , \quad (4)$$

where $\| \ \|_2^2$ is a squared l_2 norm.

Tikhonov regularization is applied by solving the following equation for ill-condition problems:

$$\mathbf{z} = \arg\min \left\{ \|\mathbf{p} - \mathbf{Mz}\|_2^2 + \lambda \|\mathbf{Lz}\|_2^2 \right\} , \quad (5)$$

where $\lambda > 0$ is the regularization parameter and $\mathbf{L}$ is the regularization operator. Since Eq. (6) may be solved using the LSQR algorithm, it may be applied to matrices that are significantly larger than those on which truncated-singular-value-decomposition (TSVD) may be practically applied, facilitating the reconstruction of high-resolution images. The L-curve method was used to find the Tikhonov regularization parameter λ. [6]

3. METHODS

After doing wavelet packet (WP) decomposition to Eq. (3), for a given leaf i or spatial frequency band in object decomposition space, the corresponding relation is [7]

$$\mathbf{p}_w^i = \mathbf{M}_w^i \mathbf{z}_w^i . \quad (6)$$

The matrix $\bar{\mathbf{M}}_w^i$ and vector $\bar{\mathbf{p}}_w^i$ are calculated out of $\mathbf{M}_w^i$ and $\mathbf{p}_w^i$ for each leaf by keeping only the significant rows. Then we can obtain

$$\bar{\mathbf{p}}_w^i = \bar{\mathbf{M}}_w^i \mathbf{z}_w^i . \quad (7)$$

For each frequency band, singular-value-decomposition (SVD) is performed on the corresponding matrix $\bar{\mathbf{M}}_w^i$ and a set of singular values is obtained: $\left\{\sigma_j^i\right\}_{j=1\ldots J}$. We introduce for each matrix $\bar{\mathbf{M}}_w^i$ a condition number that is calculated *globally*:

$$\kappa_{\mathrm{glob}}^i \left(\bar{\mathbf{M}}_w^i\right) = \frac{\mathbf{max}_{i,j}\left(\left|\sigma_j^i\right|\right)}{\mathbf{min}_j\left(\left|\sigma_j^i\right|\right)} \quad (8)$$

The use of $\kappa_{\mathrm{glob}}^i \left(\bar{\mathbf{M}}_w^i\right)$ enables classifying the different spatial frequency bands based on their reconstruction robustness. We also introduce a single *global* threshold in this work, defined as follows:

$$\mathrm{th}_{\mathrm{glob}} = \alpha \mathbf{max}_{i,j}\left(\left|\sigma_j^i\right|\right) \quad (9)$$

Once the inversion of Eq. (3) has been performed for all i, the recovered image coefficients in the WP domain $\mathbf{z}_w^i$ may be transformed. Mathematically, this reconstruction procedure may use the following equation:

$$\mathbf{z}_0 = \bar{\mathbf{M}}^\dagger \mathbf{p} , \quad (10)$$

where $\bar{\mathbf{M}}^\dagger$ is the approximated inverse matrix of $\bar{\mathbf{M}}$, and $\mathbf{z}_0$ is the approximated solution. The initial approximation may be improved recursively by using

$$\mathbf{z}_n = \mathbf{z}_{n-1} + \beta \bar{\mathbf{M}}^\dagger (\mathbf{p} - \mathbf{Mz}_{n-1}) , \quad (11)$$

where $\mathbf{z}_n$ is the solution at the nth iteration and β is a constant parameter.

4. RESULTS

The ability to perform SVD on the reduced matrices $\bar{\mathbf{M}}_w^i$ enables us to analyze the reconstruction stability for the different spatial frequency bands in the image. Two-level WP decomposition is performed, leading to 16 distinct spatial frequency bands, as depicted in Fig. 1(a). $\mathbf{A}$ represents the approximation components of the image, which are achieved via low-passing, whereas $\mathbf{D_1}$, $\mathbf{D_2}$ and $\mathbf{D_3}$ represent the detail components which are achieved via high-passing. Figs. 1(b-d) show the value of $\kappa_{\mathrm{glob}}^i \left(\bar{\mathbf{M}}_w^i\right)$ for the various frequency bands for a point detector, and line detectors with lengths of 6 mm and 13 mm, respectively. As expected, the effect of spatial averaging reduces the reconstruction stability in the higher spatial frequencies. Fig. 1(e) shows the value of the maximum global condition number of the reduced modal matrices $\mathbf{max}_i\left[\kappa_{\text{glob}}^i\left(\bar{\mathbf{M}}_w^i\right)\right]$ for various detector lengths. Interestingly, $\mathbf{max}_i\left[\kappa_{\text{glob}}^i\left(\bar{\mathbf{M}}_w^i\right)\right]$ does not monotonically increase with detector length, but rather reaches a maximum value at a length of 6 mm.

GWP-IMMI-FAD was demonstrated on experimental optoacoustic data of microspheres (100 μm). The microspheres reconstruction was set with the size of 2 cm$\times$2 cm and 200×200 pixels. All reconstructed images were normalized to its maximum and negative values in the images were set to zero. Figs. 2(a-d) respectively show the full view reconstructions of microspheres obtained by BP, IMMI, IMMI with finite-aperture detectors (IMMI-FAD) and GWP-IMMI-FAD. In GWP-IMMI-FAD, TSVD was used where truncation was performed using $\alpha = 0.15$ in Eq. (12). After all the matrices had been pre-calculated, the reconstruction using GWP-IMMI-FAD with 10 iterations took only 80 s, whereas the IMMI-FAD reconstruction required 1646 s.

Figs. 3(a-d) respectively show the full view reconstructions of the mouse brain obtained by BP, IMMI, IMMI-FAD and GWP-IMMI-FAD. The microspheres reconstruction was set with the size of 1.2 cm$\times$1.2 cm and 120×120 pixels. TSVD was used in GWP-IMMI-FAD where truncation was performed using $\alpha = 0.08$ in Eq. (12). Clearly, the reconstruction achieved by the model matrices which included the effect of the line-segment detectors was sharper than the reconstruction of point detectors. In contrast, the difference between Fig. 3(c) and Fig. 3(d) was small and could hardly be detected by visually inspecting the reconstructions. After all the matrices had been pre-calculated, the reconstruction using GWP-IMMI-FAD with 10 iterations took only 11 s, whereas the IMMI-FAD reconstruction required 197 s.

5. DISCUSSIONS & CONCLUSIONS

In this paper we develop GWP-IMMI-FAD, which is the generalization of the WP framework to finite-aperture detectors. Under the WP framework, the image is divided into a set of spatial frequency bands that are individually reconstructed from only a fraction of the projection data, leading to a set of reduced model-matrices. This approach enables the use of TSVD to obtain a regularized inverse matrix to the tomographic problem. In contrast, inversion of the originating model matrix cannot be generally performed using TSVD for high resolution images owing to the prohibitively large matrix size. Therefore, regularization requires applying iterative optimization algorithms, which are characterized by significantly higher run time. One notable improvement in GWP-IMMI-FAD over the original WP framework, developed for point detector, is the introduction of a global threshold for TSVD. As a result, GWP-IMMI-FAD applies also to cases in which some spatial frequency bands in the imaged object are impossible to reconstruct.

The application of GWP-IMMI-FAD for image reconstruction was showcased for experimental optoacoustic data. In all examples, the model matrix was too large for applying TSVD directly on it, and Tikhonov regularization was used instead. However, the reduced matrices in the wavelet packet decomposition were sufficiently small for performing TSVD. In case of the full view reconstruction, for both simulation and experimental data, the corresponding reconstruction quality obtained using the proposed GWP-IMMI-FAD was comparable to the one obtained using Tikhonov regularization IMMI-FAD. In all the examples studied, over an order of magnitude improvement in reconstruction time was achieved by GWP-IMMI-FAD.

The performance demonstrated in this work may prove useful for high-throughput optoacoustic imaging studies, which may require the reconstruction of thousands of cross-sectional images. Moreover, the results suggest that the WP framework is not an approach that is restricted to ideal imaging scenarios, but that it could be rather generalized to manage the effects of finite-size aperture and limited-view tomography. Further generalization may be achieved by applying this framework to geometries employing focused detectors as well as to 3D reconstruction problems, in which a greater need exists for acceleration of model-based reconstruction times. Finally GWP-IMMI-FAD may be used as a tool for optoacoustic system design. Already in this work, GWP-IMMI-FAD revealed an unknown property of systems with finite-aperture detectors: Beyond a certain detector length, further increments in length may lead not only to stronger optoacoustic signals, but also to more stable reconstructions.

REFERENCES

[1] Queiros, D., Dean-Ben, X. L., Buehler, A., Razansky, D., Rosenthal, A., and Ntziachristos, V., "Modeling the shape of cylindrically focused transducers in three-dimensional optoacoustic tomography," Journal of Biomedical Optics **18**(7), 076014 (2013).

[2] Rosenthal, A., Ntziachristos, V., and Razansky, D., "Model-based optoacoustic inversion with arbitrary-shape detectors," Medical Physics **38**(7), 4285-4295 (2011).

[3] Xu, M., and Wang, L. V., "Universal back-projection algorithm for photoacoustic computed tomography," Physical Review E **71**(1 Pt 2), 016706 (2005).

[4] Rosenthal, A., Razansky, D., and Ntziachristos, V., "Fast semi-analytical model-based acoustic inversion for quantitative optoacoustic tomography," IEEE Transactions on Medical Imaging **29**(6), 1275-1285 (2010).

[5] Kostli, K. P., and Beard, P. C., "Two-dimensional photoacoustic imaging by use of Fourier-transform image reconstruction and a detector with an anisotropic response," Applied Optics **42**(10), 1899-1908 (2003).

[6] Calvetti, D., Morigi, S., Reichel, L., and Sgallari, F., "Tikhonov regularization and the L-curve for large discrete ill-posed problems," Journal of Computational and Applied Mathematics **123**(1-2), 423-446 (2000).

[7] Rosenthal, A., Jetzfellner, T., Razansky, D., and Ntziachristos, V., "Efficient Framework for Model-Based Tomographic Image Reconstruction Using Wavelet Packets," IEEE Transactions on Medical Imaging **31**(7), 1346-1357 (2012).

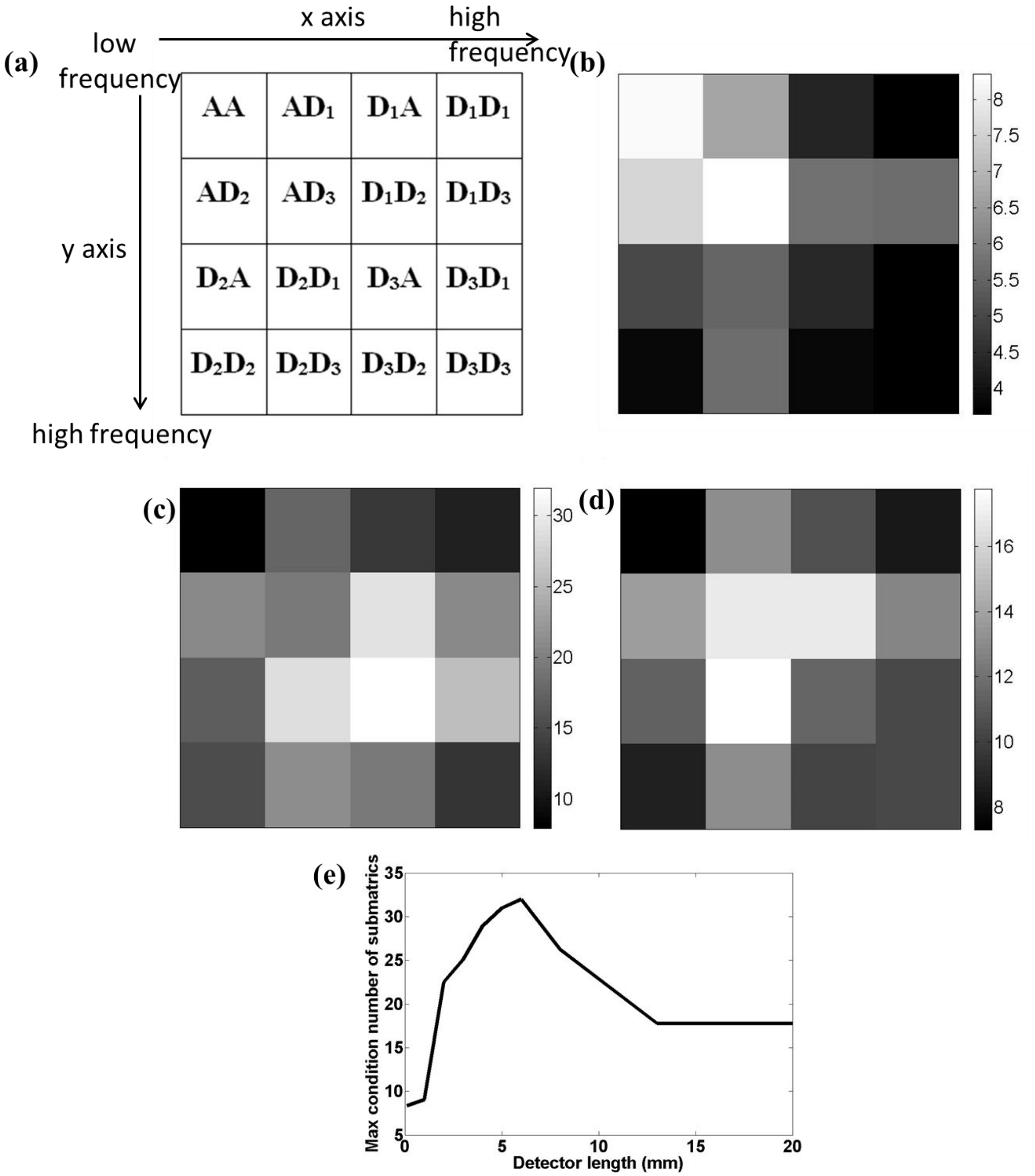

Fig. 1 (a) Decomposition components map with two level wavelet packets, (b)-(d) condition number map of decomposed model matrix of the point detector, line detectors with lengths of 6mm and 13mm, (e) maximum condition number of all decomposition matrix with different length of detectors.

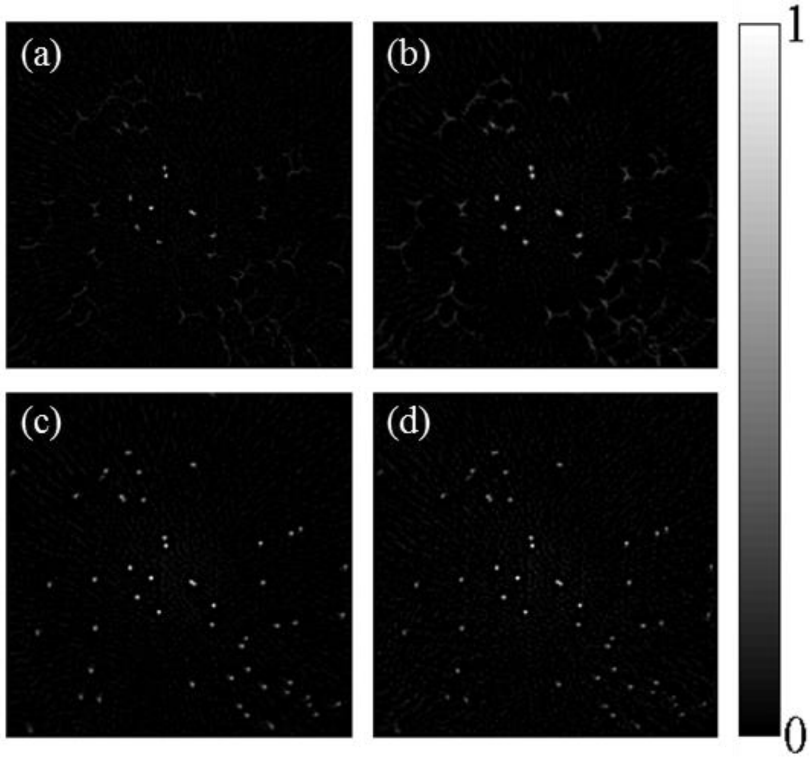

Fig. 2 Optoacoustic reconstructions of microsphere from experimental data using (a) BP, (b) IMMI, (c) IMMI-FAD and (d) GWP-IMMI-FAD.

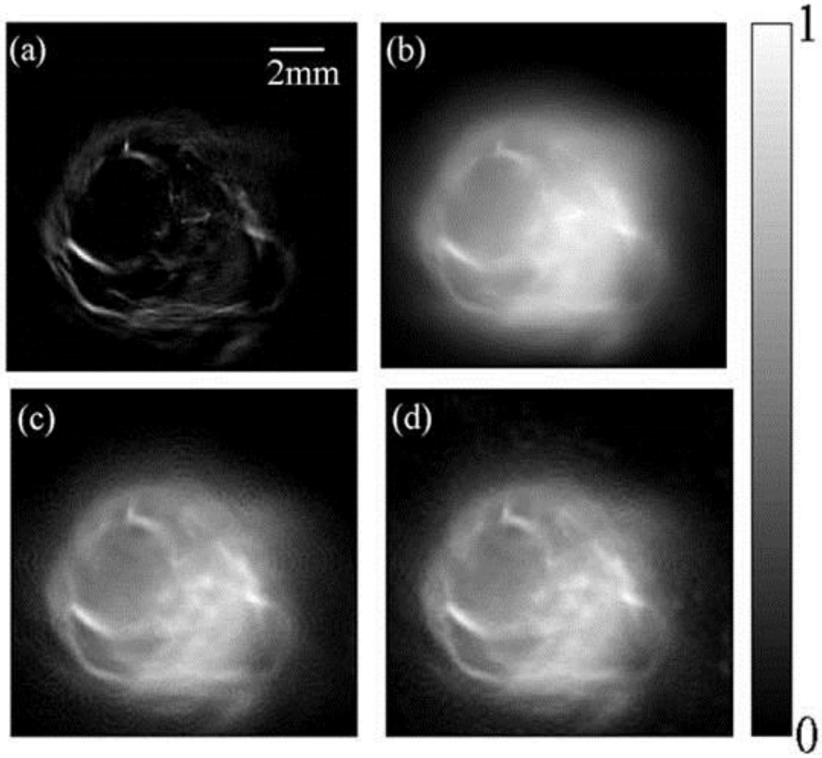

Fig. 3 Optoacoustic reconstructions of a mouse's head from experimental data using (a) BP, (b) IMMI, (c) IMMI-FAD and (d) GWP-IMMI-FAD.